Simulation of computed tomography (CT) images using a Monte Carlo approach

Anna M. Wysocka-Rabin,
Sima Qamhiyeh,
Oliver Jäkel

Abstract. Heavy ion treatment planning uses an empirical scanner-dependent calibration relation between computed tomography (CT) numbers and ion range. Any deviation in the values of CT numbers will cause a drift in the calibration curve of the CT scanner, which can reduce the accuracy of treatment beam delivery. To reduce uncertainty in the empirical estimation of CT numbers, we developed a simulation that takes into consideration the geometry, composition, and physical process that underlie their measurement. This approach uses Monte Carlo (MC) simulations, followed by a simple filtered back-projection reconstruction. The MC code used is BEAMnrc/EGSnrc. With the manufacturer's permission, we simulated the components (X-ray tube, associated filters and beam shapers) of a Siemens Emotion CT. We then generated an initial beam shape and spectra, and performed further simulations using the phantom with substitutes. We analyzed the resulting phase space file to calculate projections, taking into account the energy response of the CT detectors. Then, we applied a simple reconstruction algorithm to the calculated projections in order to receive the CT image.

Key words: X-ray tomography • Monte Carlo (MC) method • treatment planning • hadrontherapy

A. M. Wysocka-Rabin✉
Department of Accelerator Physics,
The Andrzej Sołtan Institute for Nuclear Studies,
05-400 Otwock/Świerk, Poland,
Tel.: +48 22 718 0453, Fax: +48 22 779 3481,
E-mail: wysocka@ipj.gov.pl

S. Qamhiyeh, O. Jäkel
Department of Medical Physics,
German Cancer Research Centre (DKFZ),
Im Neuenheimer Feld 280,
D-69120 Heidelberg, Germany

Introduction

In X-ray CT, an X-ray source and an arc of detectors rotate around a body that is positioned in the center of rotation to record X-ray projections from different directions. The measured X-ray projections are then translated into sectional images using reconstruction algorithms [4]. The resulting CT images are used as a quantitative measure of tissue properties for radiotherapy treatment planning.

High-quality CT images are essential for precise planning of heavy ion radiotherapy procedures. Ions deposit most of their energy in a narrow region near the end of their range (Bragg peak). Therefore, radiotherapy with heavy ion beams enables high spatial accuracy of the delivered dose. The transport of ions in tissue, and thus their range of therapeutic effectiveness, depends on the electron density of the tissue, which can only be calculated from CT images.

An empirical calibration relation between CT numbers and ion range is used for treatment planning in heavy ion radiotherapy [3]. This relation is estimated as a piecewise linear relation between measured CT numbers and the range of ions in tissues and tissue-like plastic materials. The relation is dependent on the type of CT scanner and on the measurement conditions. Any variation in the measured CT numbers causes a drift in the calibration curve of the CT scanner [7]. Jäkel *et al.* [3] measured CT numbers for different tissue and relative ranges in water for carbon ions with an energy of

270 MeV per nucleon. The uncertainty of CT numbers they found was from 5 Hounsfield units (HU) for muscle tissue to 265 HU for human bone. These uncertainties resulted in a drift of the calibration curve of the CT scanner of approximately 2–3%, and, as a consequence, the uncertainty of the absolute range is 2–3 mm in 10 cm depth. To ensure accuracy higher than 1% in the generated 3-dimensional (3-D) dose plan, it is estimated that the uncertainty of the CT number should not exceed 10 HU in the soft tissue region.

The value of CT numbers depends on the following parameters:
– Scanned object (dimensions, geometry, inhomogeneity, position in the CT gantry and movement).
– CT-machine characteristics (filtration, dimensions, collimation, etc.).
– Energy of the X-ray tube in the CT machine.
– Reconstruction algorithms.

The value of measured CT numbers is also affected by the presence of image artifacts, e.g. from beam hardening or strong absorption in metals.

Some of the factors above cause a systematic deviation which could be measured and corrected for, as in the cases of X-ray tube energy, beam hardening, field of view (FOV) and reconstruction algorithms. Nevertheless, the uncertainty of the measured CT numbers in bone-like materials can be as high as 5% (300 HU).

The aim of this study was to quantify the effects of CT parameters on measured values of CT numbers and on CT number-to-range conversion relation. In this work, primary results of a MC simulation of the filters and phantoms is presented. The effect of the photon spectral distribution and energy fluence across the FOV on CT images is also discussed.

Materials and methods

In this work, a CT unit was modeled based on the design of a Siemens Somatom Emotion CT scanner. The data is protected by a non-disclosure agreement between the Siemens Medical Solutions and the Medical Physics Department of the German Cancer Research Center (DKFZ).

The MC code BEAMnrc/EGSnrc was used to model the CT scanner and a phantom with different inserts. To our knowledge, the EGSnrc MC code [5] has the most advanced electron transport algorithm of all MC codes used in medical physics in the energy range 1–150 keV [1, 6, 10].

The MC simulation investigates the propagation of X-ray photons from the X-ray tube to the detectors, and takes into account all media in their path. Then, CT images are calculated from the simulation results. A schematic diagram of the simulated system is shown in Fig. 1. Measurement using a 16 cm phantom of polymethylmethacrylate (PMMA) in the center of FOV was simulated.

General settings of MC parameters

Throughout the simulation, the photon cut-off-energy (PCUT) and the electron cut-off-energy (ECUT) were
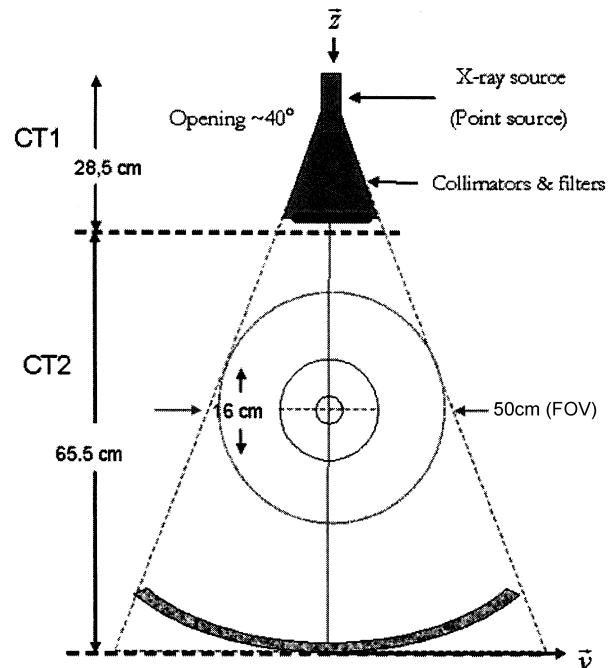

Fig. 1. Scheme of simulated CT unit and phantom.

0.001 and 0.516 MeV, respectively. These values ensure accurate electron transport of photons and secondary electrons throughout the simulation. A regional ECUT of 0.521 MeV was used in the simulation of collimators to reduced calculation time by 18%. In a simulation performed, using a monoenergetic photons source at energy of 70 keV, it was found that deactivating Rayleigh scattering in the MC simulation decreases the value of counts in the spectral distribution by up to 3% of the total signal. Similarly, introducing bound Compton scattering and electron relaxation effect affected the spectrum of simulated photons by 2 and 1%, respectively. Therefore, the simulation was performed while the following physical processes were activated: bound Compton scattering, Rayleigh scattering, atomic relaxation and relativistic spin effects. Parameter of electron transport ESTEPE is the maximum fractional energy loss per electron step. The ESTEPE was set to 0.25.

Cross-section data

The cross-section database was created by the code PEGS4. The parameters AP and AE are the low-energy thresholds for the production of secondary Bremsstrahlung photons and knock-on electrons, respectively. AP and AE should be defined lower than any used ECUT or PCUT values. Hence, AE of 0.516 MeV and AP of 0.001 MeV were used to calculate the cross-sections which define the interactions of X-ray and secondary electrons with the different simulated media. The cross-section data was also based on the elemental composition of the materials.

Geometry in MC simulation

Each hardware component was simulated as a separate unit (compound module) to allow studying the effect of individual modules on the CT image. The efficiency

of X-ray generation by electrons is very low (0.5%). Therefore, it is inefficient to simulate the CT from the tube to detectors in one run. Instead, the X-ray tube was approximated by a collimated point source with the precalculated photon spectra. The source was defined at a distance of 3.4 cm from the following simulated component. Photon spectra with a maximum energy of 80, 110 and 130 keV (manufacturers' specification) were used as input data to the point source. The spectral distributions of the three different X-ray tube voltages were calculated using the standard X-ray tube compound module of the simulation code and manufacturer's parameters. The influence of different parameters of the X-ray tube on X-ray spectra is discussed by Romanchikova [8].

Simulation of the CT hardware and phantom was divided into 2 parts, CT1 and CT2. Each part of the simulation terminated with the so-called scoring plane. A phase space file (PHSP) was calculated at each scoring plane. The simulated particles are referred to as events. Each PHSP contains data relating to energy, position, direction, charge, etc. for every event crossing a scoring plane.

The source, filters and collimator were simulated in CT1, the first part of the calculations. The modeled CT scanner has an aluminum bow-tie filter, followed by a Teflon filter. The collimator aperture was chosen to provide a field size of 50 cm by 1 cm in the centre of the CT.

The resulting PHSP is identified in this work as PHSP1. A phantom with different substitutes was simulated in CT2, the second part of the calculations. PHSP1 was used as input to the subsequent CT2 part of the calculations. The PHSP resulting from the CT2 phase of the simulation is identified in this work as PHSP2. In this phase, various phantoms with different inserts were modeled. A cylindrical phantom from PMMA was simulated using the side-tube compound module. It was designed in 3 layers, which represent the inserts (2.8 cm diameter), the phantom (16 cm diameter) and the air in the FOV (50 cm diameter), respectively. Figure 1 displays a schematic graph showing the location of the scoring planes and the simulated hardware in each part of the simulation. The number of incident particles was 10^9 and 5×10^8 photons in CT1 and CT2, respectively. To analyse the PHSP data, the BEAMDP program was used to derive photon spectral distributions and energy fluence as a function of the position in the different scoring planes on PHSP1 and PHSP2.

Reconstructing CT images from PHSP

Obtaining CT images from MC simulation results requires representation of the output of the simulation in projection-data (signal per detector element). PHSP2 is the output of the simulation at the last scoring plane which represents the detectors. The signal of each detector was calculated based on the energy and position of each photon in PHSP2 and the design parameters of the detector-arc. In a real CT machine the detectors are arrayed in an arc that is focused on the source. The detectors were considered equiangularly spaced with an angle of 27° between central and edge detectors.

The detectors were made of gadolinium oxysulfide. Their energy response function was calculated by Heismann et al. [2]. As the energy of each photon is given in the PHSP file, each photon was assigned an efficiency-weigh, which was estimated from the energy response function of the detectors [2]. Then, the photons were resampled into detector elements using the information on their position in the scoring plane. Resampling also required knowing of the number of detectors in the array, the length of the detector's active area and the dark areas between the adjacent detectors. Finally, the signal was calculated in each detector as the sum of efficiency-weighted photons.

Each CT image was reconstructed from the detector signals using an algorithm that is equivalent to the manufacturers' specifications [9]. The reconstruction algorithm was developed by Image Reconstruction Group of the Medical Physics Department of the Institute of Medical Physics in Friedrich-Alexander-University, Erlangen-Nürnberg, Germany. The code was used with the permission of developers for our specific calculations.

Figure 2 schematically summarizes the different steps used to calculate CT numbers starting from a point source with given photon spectra.

Results

Photon spectra resulting from the simulation of three X-ray tube voltages (80, 110 and 130 kV) as calculated by Romanchikova, were used as input [8]. The effect of filters was investigated in terms of the photon spectral distribution at the center and the edge of FOV. The spectral distribution resulting from transporting X-rays
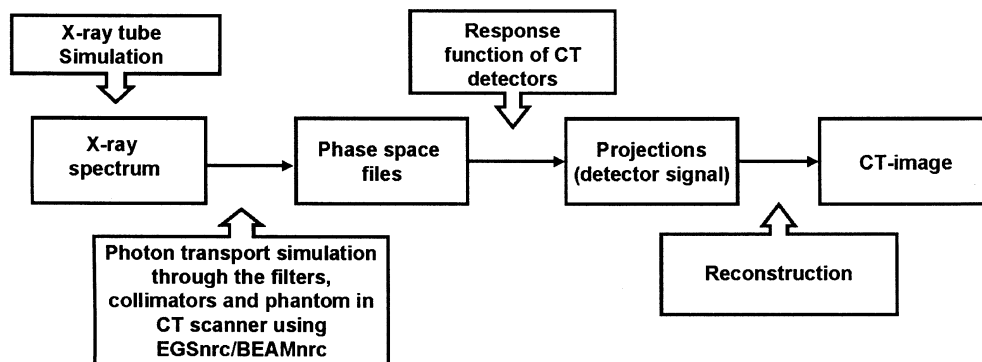

Fig. 2. Workflow to simulate CT numbers taking into consideration the geometry, composition, and physical process behind the measurement of CT numbers. The procedure starts from the X-ray tube simulation and generation of PHSP file. Then X-rays are transported through CT and phantom inserts. Finally, a CT image is reconstructed and CT numbers are calculated.
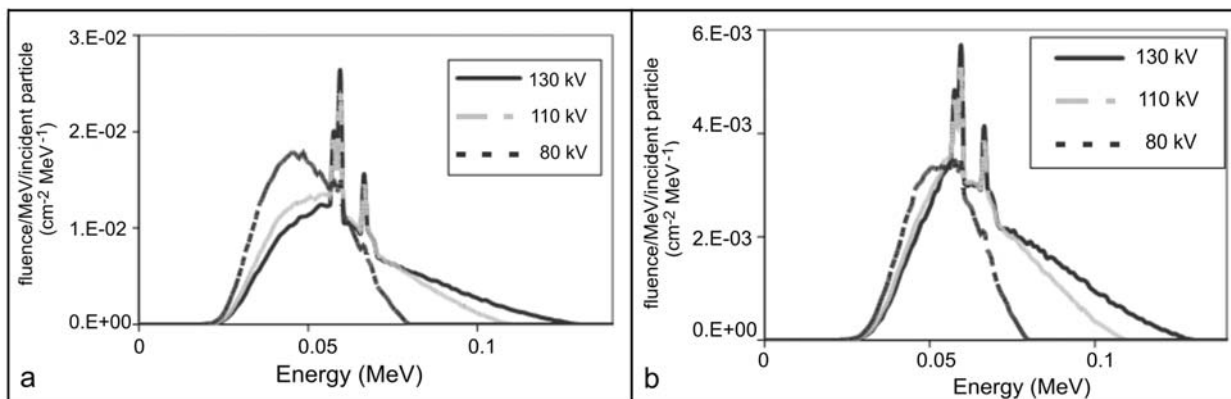
Fig. 3. Photon spectral distribution after transport through CT filters and collimator, calculated with the 3 different spectra of X-ray tube in the centre of FOV (a) and at the edge of FOV (b).
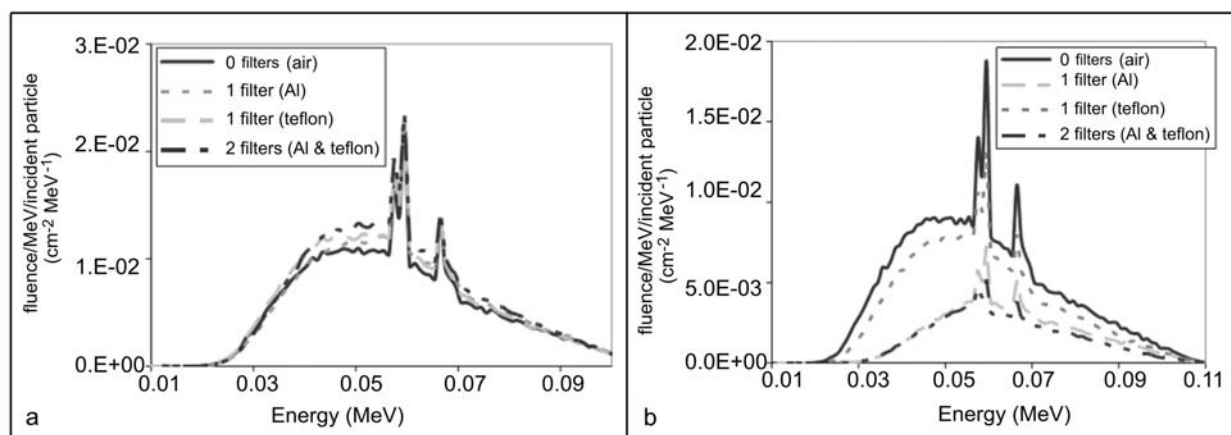

Fig. 4. Photon spectral distribution after transport through CT different filters. The spectral distribution was calculated using 110 kV X-ray spectrum from the X-ray tube simulation. The image shows the photon spectral distribution for different filters in the centre of FOV (a) and at the edge of FOV (b).

through the two filters with the three input spectra (80, 110 and 130 kV) is shown in Fig. 3a at the central axis and in Fig. 3b at the edges of FOV.

The effect of filters on the spectral distribution was also investigated by simulating the filters individually, then simulating both simultaneously. To aid in interpreting the results, a simulation where no filters (X-ray travel through air) was also performed. The spectral distribution resulting from the above simulations of different filter arrangements were carried out using 10^9 photons with an incident energy of 110 kV. The figures show a different spectral distribution depending on the length and composition of the transverse material. For simplification, only the results at the center of FOV and at the edge of FOV are presented in Figs. 4a and 4b, respectively. Figure 5 presents energy fluence vs. position, calculated for different filters arrangements and 110 keV X-ray tube voltages.

In addition, a PHSP1 in which both filters were simulated was used as the source file for the second part of calculation CT2. The 110 kV X-ray spectra were used as input to CT1 part of the simulation. PHSP2 is the result of propagation of X-rays through the phantom and different inserts. From the resulting PHSP2, spectral distribution reflecting the transport of X-rays through phantom and inserts were calculated. Energy fluence as a function of position was calculated for the cylindrical phantom with the different inserts.

Similarly, the spectral distribution for cortical bone insert and for different voltage of the incident photons (80, 110, 130 kV) is presented in Fig. 6. The energy fluence as a function of position was calculated after the
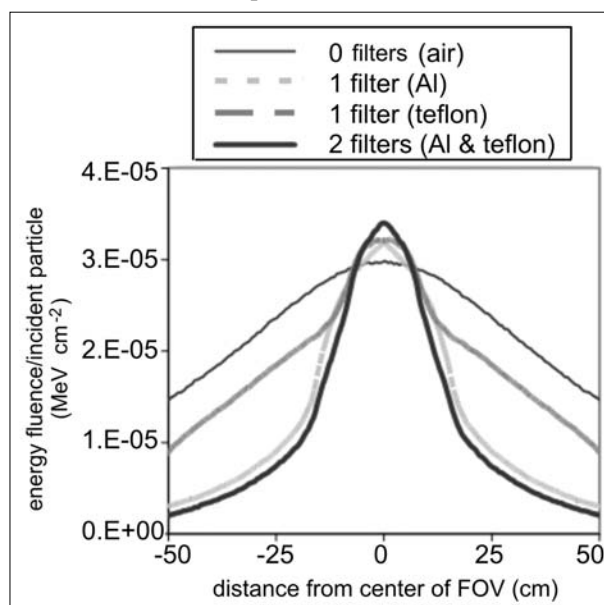

Fig. 5. Energy fluence vs. position due to different filters. The results were calculated using the spectrum simulating 110 kV X-ray tube voltage.
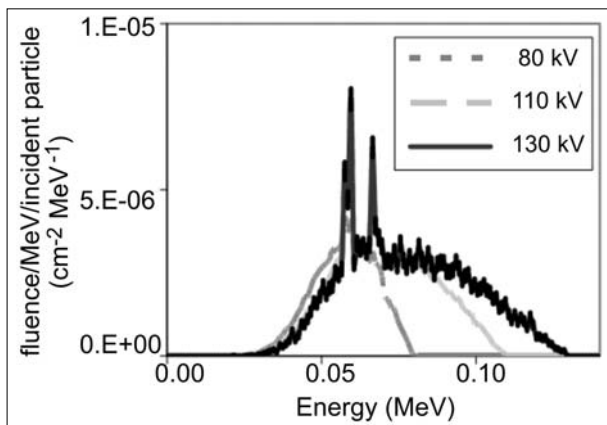
Fig. 6. Comparison of spectral distribution after transport of X-rays through cortical bone insert for different X-ray spectra (80, 110, 130 kV).

Fig. 8. Reconstructed image of the plexiglas phantom with cortical bone. Axis are pixel index for a 512×512 pixel image and a FOV of 50 cm diameter.

cylindrical phantom with cortical bone insert for the three incident photon energies (Fig. 7).

The number of events used as a source in the CT1 part of the simulation strongly affects the uncertainties of the results in PHSP2. This uncertainty increased with the number of times that PHSP1 was recycled. The PHSP is also recycled when the number of requested events is less than the statistics available in PHSP. The statistical uncertainty was reduced by 50% when the number of initial particles from the source was increased from 10^8 to 10^9 photons in CT1. For the results shown in Figs. 3–7, the number of incident particles in the first part of the simulations was 10^9 and the number of incident particles in the second part of the simulation was 5×10^8.

An example of the reconstructed image of the Plexiglas phantom with a cortical bone insert is presented in Fig. 8.

In this work, PHSP1 was, on average, recycled 4 times to produce the required photon events requested in CT2. Most events were lost at the collimator.

Discussion

The attenuation of the photons in the filters is stronger towards the edge of the FOV. The spectral distribution of mean energy of the incident photons increases with distance from the center of the FOV as the filtration
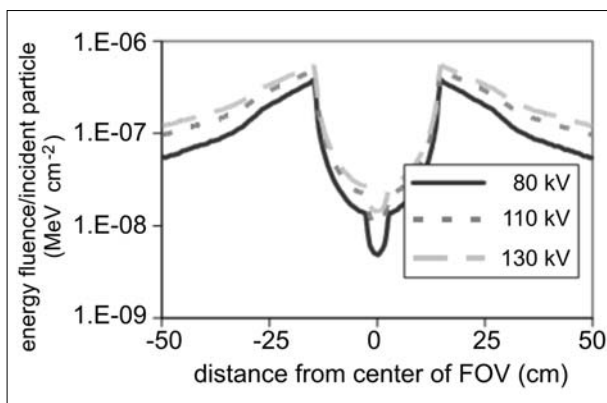

Fig. 7. Comparison of energy fluence vs. position after transport through phantom with cortical bone insert. The X-ray spectra simulating the X-ray tube voltage (80, 110, 130 kV) were used.
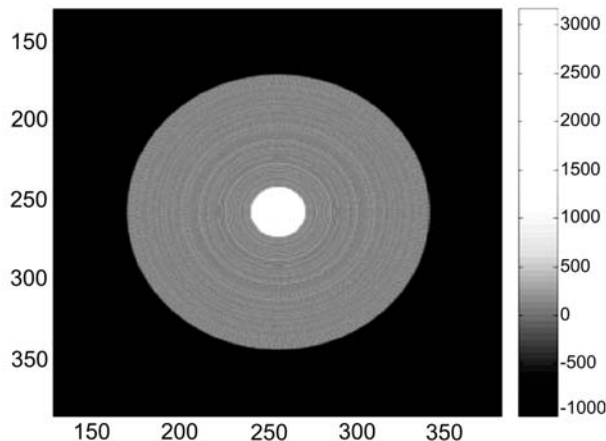
increases (Fig. 3). For 110 kV incident photons, the mean energy is 58.7 keV in the center of FOV and increases to 66.5 keV at the edge.

The filters cause beam hardening towards the edge of the FOV. The filters also focus the incident beam to the center of the FOV as seen in Fig. 5, especially by the aluminum bow-tie filter.

Less filtration of the X-rays in the center of FOV is necessary to produce CT pictures with good resolution where the patient's body is expected to be thickest. Furthermore, as the mean energy of X-rays increases, the deposited dose in the measured objects is reduced. At the edge of the FOV, the patients' bodies are not expected to be thick and the attenuation of X-rays is less. Therefore, the increased beam hardening of the X-ray is favorable near the edge of the FOV, which permits a reduced X-ray dose without affecting the quality of CT images. Figure 3 shows the expected spectra in the FOV.

The spectral distribution of an X-ray beam, which is calculated after the phantom with different inserts, depends strongly on the initial spectrum and the electron density of the inserts. Though the information is not shown here, the spectrum is significantly shifted to higher energies (beam hardening) for higher electron densities of the insert material. Although this knowledge is important, it cannot be obtained in clinical CTs as their current detectors do not detect photon energy as well as intensity. Therefore, we calculated beam hardening based on the assumption that all material attenuates X-rays similarly to water. Although this is a crude assumption, it is still valid for patients as water comprises the main part of tissue composition.

The energy fluence that is calculated after the phantom with the inserts shows how the insert material attenuates the photon beam in comparison to the PMMA phantom and the surrounding air. This change in attenuation is translated into change in the projection data and the CT numbers. The effect of X-ray tube voltage on the value of the attenuation is also clear from Fig. 7.

Lower energy of the incident photons results in more attenuation and a higher dose to the patient. This is also translated into higher CT numbers in the CT images that were calculated from the projections.

In Fig. 8, the statistical uncertainties in these projections are large. However, since only a few projections are simulated into CT images, the fluctuations become strongly correlated and are translated into ring artifacts as seen in Fig. 8. The effect of these artifacts on CT numbers is an uncertainty in the simulated numbers, which is of the order of 200 HU. In subsequent work, we reconstructed images from several simulated projections, as opposed to the single projection described in the work reported here. In a clinical CT scanner, around 1000 independent projections are reconstructed into a single CT image.

Conclusions

This work demonstrates that the presented approach can be used to study CT images in light of physical processes. The suggested MC approach preserves the information on energy spectrum and fluence. However, improvement of the efficiency of the simulation is needed in order to study the effect of different parameters on CT numbers. Further work which investigates using different phantom materials, varying phantom size and studying the quantitative effects of CT numbers will soon be published.

References

1. Das IJ, Chapman J, Verhaegen F, Zellmer D (1999) Interface dosimetry in kilovoltage photon beams. In: Ma C-M, Seuntjens J (eds) Kilovoltage X-ray beam dosimetry for radiotherapy and radiobiology. Medical Physics Publishing, Madison, WI, pp 239–259
2. Heismann BJ, Leppert J, Stierstorfer K (2003) Density and atomic number measurements with spectral X-ray attenuation method. J Appl Phys 94;3:2073–2079
3. Jäkel O, Jacob C, Schardt D, Karger CP, Hartmann GH (2001) Relation between carbon ion ranges and X-ray CT numbers. Med Phys 28;4:701–703
4. Kalender WA (2000) Computed tomography: fundamentals, system technology, image quality, applications. John Wiley & Sons, New York
5. Kawrakow I, Rogers DWO (2001) The EGSnrc code system: Monte Carlo simulation of electron and photon transport. Report no. PIRS-701. National Research Council of Canada, Ottawa
6. Marianno CM, Higley KA, Palmer TS (2000) A comparison between default EGS4 and EGS4 with bound Compton cross-sections when scattering occurs in bone and fat. Health Phys 78;6:716–720
7. Qamhiyeh S, Wysocka-Rabin A, Ellerbrock M, Jäkel O (2007) Effect of voltage of CT scanner, phantom size and phantom material on CT calibration and carbon range. Radiother Oncol 84;S1:S232
8. Romanchikova M (2006) Monte Carlo Simulation des Röntgenspektrumseiner computertomographischen Röntgenröhre. Master's thesis, University of Heidelberg, Germany
9. Sennst A, Kachelriess M, Leidercker C, Schmidt B, Watzke O, Kalender WA (2004) An extensible software--based platform for reconstruction and evaluation of CT images. Radiographics 24;2:601–613
10. Verhaegen F (2002) Evaluation of the EGSnrc Monte Carlo code for interface dosimetry near high-Z media exposed to kilovolt and ^{60}Co photons. Phys Med Biol 47:1691–1705